Characteristics of Edge-Emitting Bragg Reflection Waveguide Lasers

Cunzhu Tong, *Member, IEEE*, Bhavin J. Bijlani, Sanaz Alali, and Amr S. Helmy, *Senior Member, IEEE*

***Abstract*— We demonstrate experimentally the stable continuous-wave (CW) single-mode operation of Bragg reflection waveguide (BRW) lasers from 10 to 100 °C. The threshold characteristics, quantum efficiency, gain, and self-heating characteristics are investigated in detail. Threefold enhancement in the optical confinement is achieved using these BRW structures for a core width two times that of their edge-emitting total internal reflection counterparts. The device shows also the high gain and characteristic temperature (∼197 K) under CW operation from 10 to 100 °C. The mode stability is analyzed by the calculated mode reflection spectrum, injection-current-dependent lasing spectrum, and near-field patterns.**

***Index Terms*— Anti-guided lasers, Bragg reflection waveguides, high-power lasers, semiconductor lasers, threshold.**

I. Introduction

EDGE-EMITTING Bragg reflection waveguide (BRW) lasers are essentially 1-D photonic bandgap (PBG) p-i-n structures, where light is guided by Bragg reflectors with light propagating parallel to the epi-layers [1], [2]. They have recently attracted much attention due to their unique merits, in particular structures where the core is the layer of the lowest refractive index in the structure. In such a configuration, vertical guiding based solely on bandgap effects can be achieved, enabling large core dimensions, while maintaining single-mode operation. Other predicted advantages include large mode volumes [3], [4], high gain coefficient [5], and strong mode discrimination, allowing stable single-mode operation [4], [6], [7]. Moreover, the most significant advantage of this class of lasers is their compatibility with waveguide structures with capabilities of efficiently phase-matching second-order nonlinearities within the laser cavity [8], [9]. This novel capability can enable unique applications related to nonlinear frequency conversion [10], [11] and opto-electronic integrated circuits, such as monolithic electrically injected optical parametric oscillators (OPOs) and compact spontaneous parametric down-conversion single-photon and entangled-pair sources. In these devices, the BRW structures can be used as both the pump laser and the nonlinear waveguide.

Manuscript received March 12, 2010; revised May 28, 2010 and June 15, 2010; accepted June 20, 2010. Date of current version August 24, 2010. This work was supported by the Natural Sciences and Engineering Research Council of Canada.

The authors are with the Edward S. Rogers, Sr. Department of Electrical and Computer Engineering, University of Toronto, Toronto, ON M5S3G4, Canada (e-mail: cz.tong@utoronto.ca; b.bijlani@utoronto.ca; Sanaz.alali@utoronto.ca; a.helmy@utoronto.ca).

Color versions of one or more of the figures in this paper are available online at http://ieeexplore.ieee.org.

Digital Object Identifier 10.1109/JQE.2010.2055042

From a structural standpoint, BRW lasers can be viewed as a hybrid between conventional total internal reflection (TIR) edge emitters and vertical-cavity surface-emitting lasers (VCSELs). Hence, these lasers can potentially capitalize on the benefits of both classes. BRW lasers can be designed to achieve the mode selection offered by VCSELs and the high output power performance offered by large-optical-cavity TIR lasers. BRW lasers can also be extended to two dimensions by fabricating periodic structures along the lateral direction [5]. Excessive scattering losses due to fabrication imperfections may limit the benefits from extending this approach to two dimensions, though.

Many promising applications of BRW lasers are based on these structures as being part of a high-power single-mode device. However, BRW laser structures pose challenges for high-power operation due to the thick epitaxial layers, which require challenging thermal management. In turn, significant optimization and hence laser performance characterization is necessary. Recently, we have demonstrated the first double-sided 1-D BRW edge-emitting laser (EEL) [12], which shows the single transverse mode operation with low threshold current density. In this paper, we investigate in detail the threshold, mode confinement, gain, and self-heating characteristics of this new class of lasers under continuous-wave (CW) operation. In addition, performance optimization of this class of lasers is discussed. The paper is organized as follows. In Section II, the design principles and mode selection of BRW lasers are summarized. In Section III, the threshold characteristics, modal and gain characteristics, as well as self-heating characteristics of BRW lasers are presented. Conclusions are summarized in Section IV.

II. Laser Design and Fabrication

As shown in Fig. 1(a), the BRW laser consists of a low-index core layer placed between two distributed Bragg reflectors. Each Bragg reflector is made up of mutilayer stacks of alternating materials with refractive indices $n_h, n_l (n_h > n_l)$ and thicknesses d_h, d_l, respectively. The index of the core layer is $n_c (n_h > n_l > n_c)$ and thickness is d_c. The low-index core layer can ensure that the devices operate at the BRW mode and not the TIR mode. The gain is provided from quantum wells (QWs), which are located at the center of the core layer. Fig. 1(b) shows the light transmission in the BRW laser. The angle of incidence θ_c covers a range from 0 to $\pi/2$, and can be expressed as [2]

$$n_{eff} = n_c \sin \theta_c \tag{1}$$

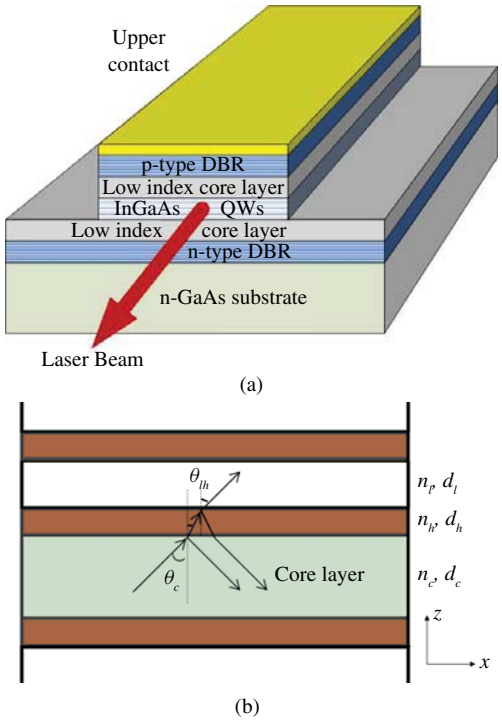

Fig. 1. (a) Schematic diagram of the BRW laser structure and (b) light transmission in the BRW laser.

where n_{eff} is the effective index of guide mode. If the Bragg reflectors provide quarter-wave optical thickness, then the n_{eff} is given by [1]

$$n_{eff} = \sqrt{n_c^2 - [(2m-1)\lambda/2d_c]^2}, \quad (m = 1, 2 \ldots) \qquad (2)$$

where m is an integer that corresponds to the mode order and hence the number of peaks in the z direction. λ is the wavelength of the BRW mode. We select $Al_{0.3}GaAs_{0.7}As/GaAs$ ($n_l/n_h = 3.34/3.512$) as the materials for the Bragg reflectors and $Al_{0.37}GaAs_{0.63}As$ as the core layer ($n_c = 3.304$) with a thickness of 700 nm. This renders the effective refractive indices n_{eff} of fundamental mode ($m = 1$) and first higher order mode ($m = 2$) to be 3.2 and 2.6, respectively. The corresponding incidence angles θ_c are 78.2° and 52.1°, respectively. There are no transverse modes with $m > 2$ in this BRW laser. The thicknesses of the Bragg reflectors can be calculated by the condition of quarter-wave BRW

$$d_{h(l)}\sqrt{n_{h(l)}^2 - n_{eff}^2} = \lambda/4. \qquad (3)$$

The equation dictates the thicknesses of GaAs and $Al_{0.3}GaAs_{0.7}As$ to be 167 and 281 nm, respectively. To examine the mode confinement, the transverse electric mode reflectivities of the structure with eight pairs of quarter-wave $Al_{0.3}GaAs_{0.7}As/GaAs$ Bragg reflectors were calculated by using the transfer-matrix method [13], which are shown in Fig. 2. It can be seen that the mode reflectivity of the fundamental transverse mode ($m = 1$) is nearly 100% at the gain wavelength of the InGaAs QWs ($\sim$980 nm). However, the corresponding reflectivity of first high-order transverse mode ($m = 2$) is only 20%. Therefore, these structures show strong transverse mode selection, which assists stable single transverse-mode operation.

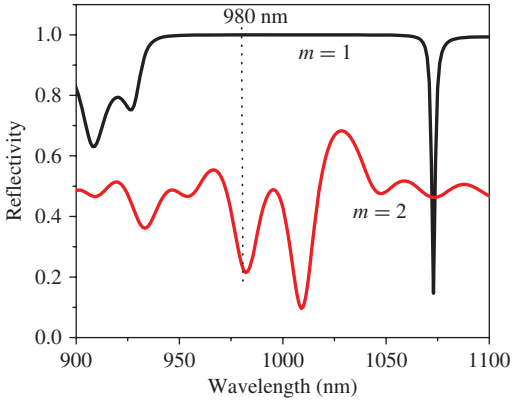

Fig. 2. Mode reflectivities of the fundamental transverse mode ($m = 1$) and the first high order mode ($m = 2$) along the z direction.

The laser structure was grown on (100)-oriented, n^+ GaAs substrate by metal-organic chemical vapor deposition. Two 6-nm $In_{0.2}Ga_{0.8}As$ QWs separated by 2-nm GaAs were grown at the center of the $Al_{0.37}Ga_{0.63}As$ low-index core layer. The upper and lower mirrors consisted of eight pairs of $Al_{0.3}Ga_{0.7}As/GaAs$ quarter-wave layers. The upper mirror was doped with carbon at 5×10^{17} cm^{-3} for the first three periods and then 10^{18} cm^{-3} for the final five periods. The lower mirror was doped with Si at 1.2×10^{17} cm^{-3} for the first three periods and then 1.2×10^{18} cm^{-3} for the final five periods. The interfaces between GaAs and $Al_{0.3}GaAs_{0.7}As$ were linearly graded in composition over 25 nm to reduce the electrical resistance. The total thickness of epi-layer was about 8.5 μm.

The samples were patterned into ridge waveguide lasers with ridge widths of 3.2 μm by dry etching. Insulation using SiO_2 and metallization defined the p-side contact. The etching depth was $\sim$3.6 μm. The samples were cleaved into laser bars and mounted on copper heat sinks with p-side up for measurement without any facet passivation or coating. The temperature of the heat sink was controlled with a thermoelectric cooler. A 7-mm diameter silicon photodiode and an Agilent 86146B optical spectrum analyzer were used to measure the output power and the lasing spectra, respectively.

III. Results and Discussion

A. Threshold Characteristics

Fig. 3 shows the CW temperature-dependent power–current (L–I) curves of a representative laser. The cavity length of the device is 0.51 mm. The threshold current I_{th} is 12.6 mA at 10 °C, i.e., the threshold current density is $\sim$772 A/cm^2, and increases to 20.5 mA at 100 °C, which is approximately 88 μA/°C. The y-axis on the right in Fig. 3 shows the voltage–current curve measured at 20 °C. The threshold voltage is $\sim$2.6-V. The high threshold voltage can be attributed to the high series resistance at heterostructure interfaces of the Bragg stack, which can be further optimized for low resistance performance. This can be achieved using standard techniques such as modulation doping [14] or superlattice structures [15].

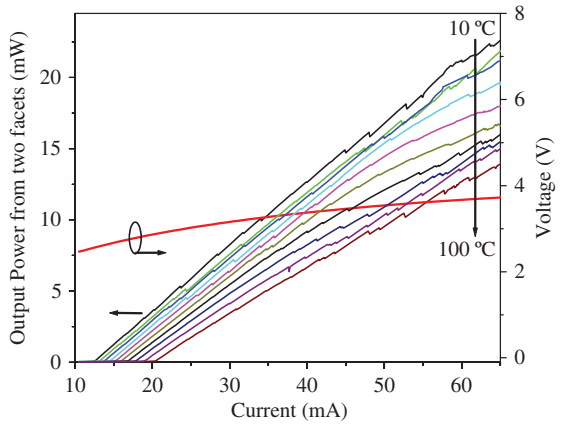

Fig. 3. CW *L–I–V* (10–100 °C) characteristics of a BRW laser.

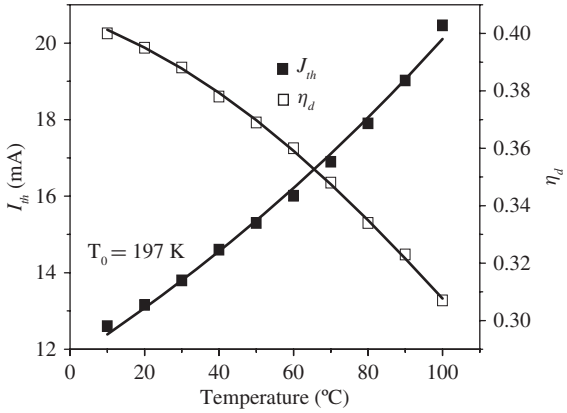

Fig. 4. Temperature dependence of threshold current density (solid squares) and external differential quantum efficiency (hollow squares). The solid lines are the theoretical fits to the data.

Fig. 4 shows the temperature-dependent threshold current (solid squares) and external quantum efficiency η_d (hollow squares). The solid lines are the curve-fitting of the results. For the threshold current (solid squares), the fitting is based on the equation $I_{th} = I_0 \exp(T/T_0)$, where T_0 is the characteristic temperature, which was found to be 197 K in the temperature range from 10 to 100 °C. The external differential quantum efficiency of the BRW laser is 0.4 at 10 °C and reduces to 0.31 when the temperature increases to 100 °C. To better understand the temperature behavior of the quantum efficiency, further analysis was carried out. The external differential quantum efficiency can be described by the well-known equation $\eta_d = \eta_i \alpha_m/(\alpha_i + \alpha_m)$, where η_i, α_i, and α_m are the internal quantum efficiency, internal loss, and mirror loss, respectively. The internal quantum efficiency of InGaAs QW lasers at threshold can be expressed as [16]

$$\eta_i = \left[1 + \frac{t_{bw}}{t_b} + \frac{t_{bw}}{t_{ewb}}\frac{t_w}{t_b}\right]^{-1} \tag{4}$$

where t_{bw} is the carrier transport time from the doped AlGaAs cladding layer to the QW, and is in the order of picoseconds. Also, t_{ewb} is the carrier escape time from the QW to the barrier [17]. In addition, t_b and t_w are the carrier recombination lifetimes in the barrier and the QW, respectively. In general, t_b and t_w are in the order of nanoseconds and depend on the current density. Here, it is assumed that t_b and t_w have weak temperature dependence at threshold due to the low temperature sensitivity of the threshold current. Meanwhile, for these calculations, we ignore the temperature dependence of both the internal loss and the mirror loss at threshold. From the definition of t_{bw} and t_{ewb} [16], [17], the temperature-dependent external quantum efficiency η_d can be expressed as

$$\eta_d^{-1} = 1 + \alpha_i/\alpha_m + aT^{1.1} + bT^{1.6}\ \exp(-E_b/k_BT) \tag{5}$$

where a, b are the temperature-independent constants, and k_B, T are the Boltzmann constant and temperature, respectively. Also, E_b is the effective confinement of the barrier. The term of $aT^{1.1}$ can be ignored because $t_{bw} \ll t_b$. From the fitting, the internal loss α_i is found to be ~ 34.2 cm^{-1} and $E_b \sim 0.152$ eV. The high loss might be due to the scattering loss of the rough sidewall and narrow ridge formed during fabrication by dry etching [18].

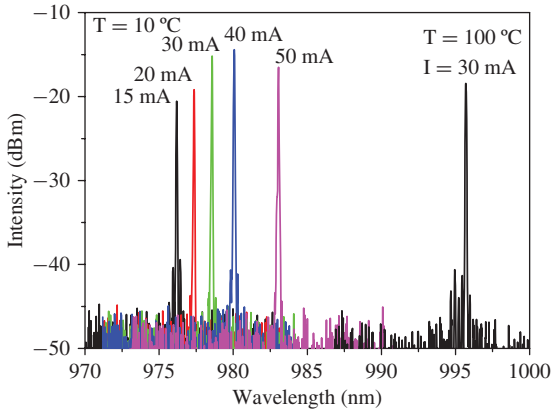

Fig. 5. CW lasing spectra of the BRW laser measured at 10 and 100 °C.

B. Mode and Gain Characteristics

The lasing spectra at different injection currents were measured and are plotted in Fig. 5. Single-mode lasing was achieved at 10 and 100 °C with the side mode suppression ratios of 30 and 23 dB, respectively. The lasing wavelength exhibits a red shift with increase in injection current, which is 7.1 nm at 10 °C for an injection current of 50 mA. Fig. 6 shows the near-field profiles measured at different injection currents. By comparing the profiles shown in Fig. 6 with the calculated near-field patterns for BRW [12], and the unique two lobes of far-field distribution [Fig. 6(e)], it can be concluded that the BRW lasers studied here lase in the BRW mode. It is notable that the near field does not undergo significant change as the current increases, confirming the selectivity of the BRW modes, as discussed in the previous section. Achieving lasing in the BRW mode enables access to laser structures where both pump lasers and second-order nonlinearities can be combined in the same cavity, where phase matching is readily available.

The sub-threshold emission spectra [inset in Fig. 7(a)] were measured from 10 to 50 °C and used to extract the net peak modal gain by using the Hakki–Paoli method [19], and are plotted in Fig. 7(a). The modal gain at 10 °C shows the highest

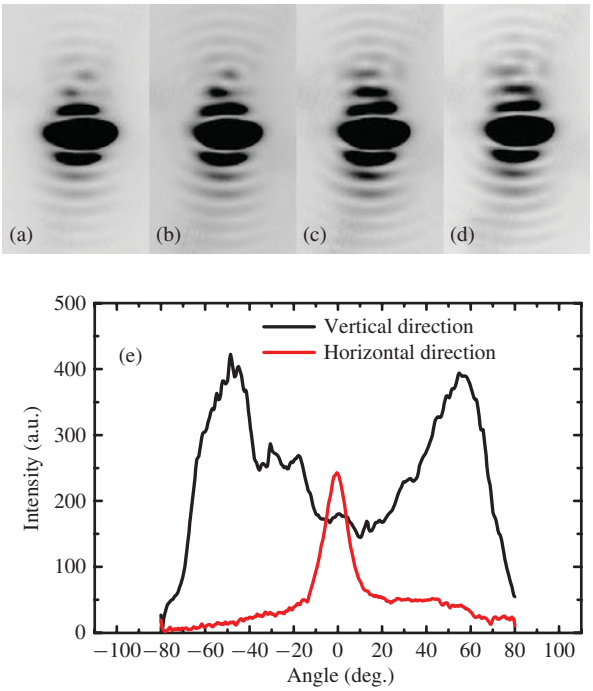

Fig. 6. Near-field profile of the BRW mode measured at 10 °C with the injection current of (a) 20 mA, (b) 30 mA, (c) 40 mA, and (d) 50 mA. (e) Far-field profile measured at room temperature with an injection current of 30 mA.

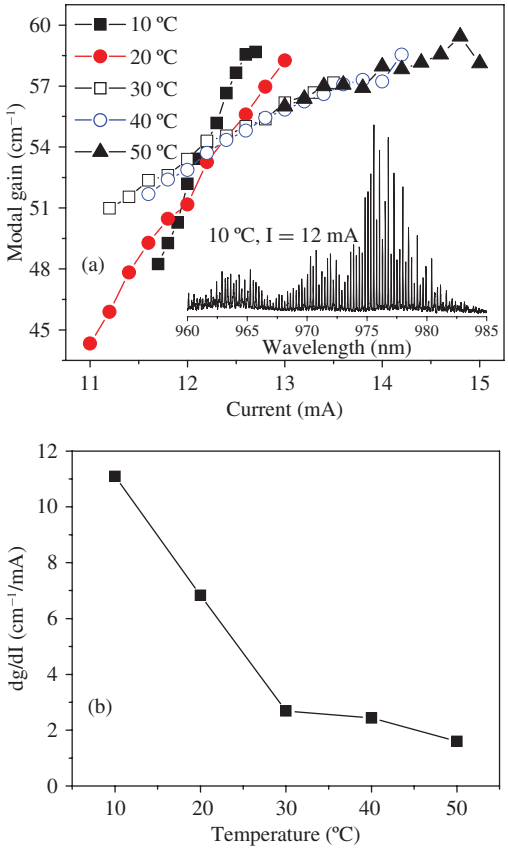

Fig. 7. (a) Modal gain vs. current at different temperatures, measured from the emission spectrum by using the Hakki–Paoli method. The inset is the typical high-resolution laser spectrum of a BRW laser measured at 10 °C with injection current of 12 mA ($0.95I_{th}$). (b) Differential gain as a function of temperature.

slope for the dependence on the current. With increase in temperature, the slopes of gain reduce and tend to plateau [Fig. 7(b)]. The core of BRW lasers can be designed several times thicker than conventional EELs while maintaining single mode action. For example, the BRW structure described here is approximately two times thicker than those of conventional EEL lasers while operating in single mode, as can be seen in Fig. 5. In general, a thicker core leads to significant reduction in the optical confinement factor (OCF) because OCF is proportional to the ratio of the QW thickness and active region thickness in the conventional TIR EEL QW lasers. So the modal gain, which is proportional to the OCF, should be low for a large-core EEL QW laser. While this holds true for TIR EEL lasers, the measured modal gain shown in Fig. 7(a) for the BRW lasers studied here is much higher than that of the typical InGaAs EEL [20]. This can be ascribed to the enhanced light confinement due to the nature of the BRW mode confinement. Theoretical calculation conducted using the mode solver software (Lumerical MODE Solutions) shows that the OCF of the BRW laser is about 5.37%, which is about three times larger than that of TIR EEL with the same active region thickness (~1.7%). This property of BRW structures represents a valuable design tool and will be explored further.

C. Self-Heating Characteristics

The lasing wavelength shift shown in Fig. 5 can be attributed to the carrier-induced bandgap shrinkage [21] and the thermally induced emission wavelength shift. The former can be obtained by the sub-threshold emission spectra at low injection currents, where the temperature variation due to self-heating can be ignored. The results are plotted in Fig. 8 as hollow squares, which show a linear current dependence of 0.014 nm/mA. The temperature dependence of the lasing mode is obtained by changing the heat sink temperature. Note that all the above measurements are focused on the same lasing longitudinal mode. As shown in Fig. 8, the thermally induced emission wavelength shift (solid squares) shows a nearly linear dependence of 0.142 nm/°C. By using the wavelength shift both due to carrier injection and to temperature change, we can estimate the temperature increase ΔT in the active region of the device according to the lasing spectrum shown in Fig. 5. The results are shown in Fig. 9. From the figure, the temperature increase is found to be 45 °C at an injection current of 50 mA with a dissipated power of 168.5 mW as extracted from Fig. 3. This leads to a thermal impedance of ~270 K/W. To ensure that this method of obtaining the temperature change in the cavity is valid, we fitted the results with the conventional empirical equation [22] $\Delta T = c_1 I + c_2 I^2$, where c_1 and c_2 are constants and I the injection current. The solid line in Fig. 9 represents the best fit using this equation. The fit agrees well with the measured data using our technique. Comparing this result with the self-heating parameter in the typical QW EEL (~100 K/W) [23] and VCSELs (~1788 K/W) [22], it is found that the self-heating effect in the BRW laser is

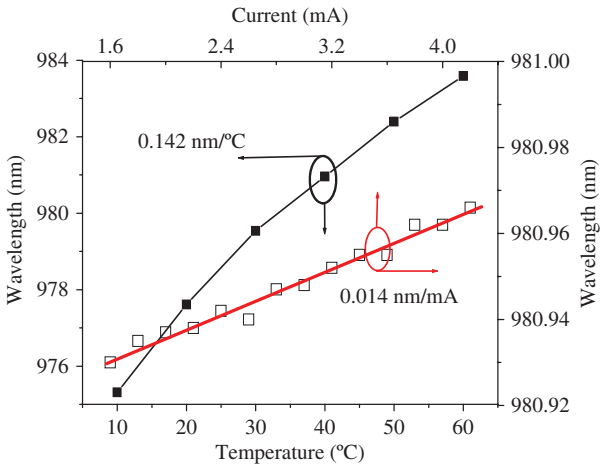

Fig. 8. Thermally induced (solid squares) and carrier-induced (hollow squares) lasing wavelength shift.

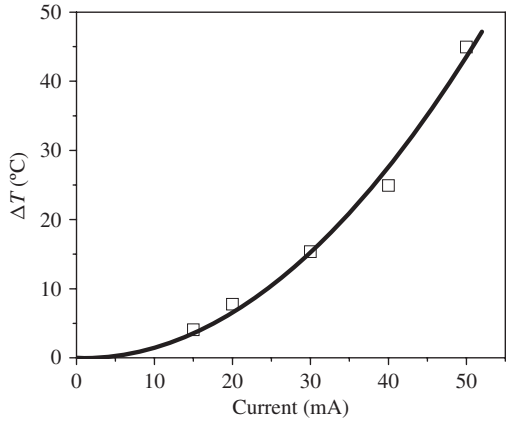

Fig. 9. Temperature increase (ΔT) in the active region of BRW lasers due to the self-heating.

higher than that in the typical EEL but much lower than in VCSELs. This is reasonable because BRW lasers are similar to VCSELs in their vertical structure, while their cavity volumes are similar to EELs. Structure optimization is expected to further reduce the thermal impedance of BRW lasers.

The square data points are obtained using the wavelength shift due to carrier injection and the wavelength shift due to temperature change. The solid line is the best fit by the empirical equation $\Delta T = c_1 I + c_2 I^2$ [22].

IV. Conclusion

We have studied the threshold characteristics, quantum efficiency, modal gain, and self-heating of a double-sided BRW laser. Optical confinement enhancement of three times that of an equivalent edge-emitting laser based on TIR was demonstrated in this BRW laser structure. This paper suggests that the BRW laser can achieve stable single transverse mode operation even at high temperature (~100 °C) with high T_0 (~197 K). We believe that these results will contribute to the optimization of BRW lasers and hence the development of compact OPOs and entangled photon sources.

V. Acknowledgment

The authors would like to acknowledge CMC Microsystems for the epitaxial growth and Prof. Hanquin of the Institute of Semiconductors, Chinese Academy of Sciences, Beijing, China, for the measurement of far-field patterns.

References

[1] B. R. West and A. Helmy, "Properties of the quarter-wave Bragg reflection waveguide: Theory," *J. Opt. Soc. Am. B*, vol. 23, no. 6, pp. 1207–1220, 2006.

[2] J. Li and K. S. Chiang, "Guided modes of 1-D photonic bandgap waveguides," *J. Opt. Soc. Am. B*, vol. 24, no. 8, pp. 1942–1950, 2007.

[3] T. H. Her, "Gain-guiding in transverse grating waveguides for large modal area laser amplifiers," *Opt. Exp.*, vol. 16, no. 10, pp. 7197–7202, 2008.

[4] W. Liang, Y. Xu, J. M. Choi, and A. Yariv, "Engineering transverse Bragg resonance waveguides for large modal volume lasers," *Opt. Lett.*, vol. 28, no. 21, pp. 2079–2081, 2003.

[5] A. Yariv, Y. Xu, and S. Mookherjea, "Transverse Bragg resonance laser amplifier," *Opt. Lett.*, vol. 28, no. 3, pp. 176–178, 2003.

[6] L. Zhu, A. Scherer, and A. Yariv, "Modal gain analysis of transverse Bragg resonance waveguide lasers with and without transverse defects," *IEEE J. Quantum Electron.*, vol. 43, no. 10, pp. 934–940, Oct. 2007.

[7] A. Mock, L. Lu, E. H. Hwang, J. O'Brien, and P. D. Dapkus, "Modal analysis of photonic crystal double-heterostructure laser cavities," *IEEE J. Select. Topics Quantum Electron.*, vol. 15, no. 3, pp. 892–900, May–Jun. 2009.

[8] B. R. West and A. S. Helmy, "Exact phase matching using Bragg reflection waveguides," *IEEE J. Select. Topics Quantum Electron.*, vol. 12, no. 3, pp. 431–446, May–Jun. 2006.

[9] A. S. Helmy, "Phase matching using Bragg reflection waveguides for monolithic non-linear applications," *Opt. Exp.*, vol. 14, no. 3, pp. 1243–1252, 2006.

[10] B. Bijlani, P. Abolghasem, and A. S. Helmy, "Second harmonic generation in ridge Bragg reflection waveguides," *Appl. Phys. Lett.*, vol. 92, no. 10, pp. 101124-1–101124-3, Mar. 2008.

[11] P. Abolghasem, J. Han, B. Bijlani, and A. S. Helmy, "Continuous wave second harmonic generation in Bragg reflection waveguides," *Opt. Exp.*, vol. 17, no. 11, pp. 9460–9467, 2009.

[12] B. Bijlani and A. S. Helmy, "Bragg reflection waveguide diode lasers," *Opt. Lett.*, vol. 34, no. 23, pp. 3734–3736, 2009.

[13] H. A. Macleod, *Thin-Film Optical Filters*. Bristol, NY: Adam Hilger, 1986.

[14] E. F. Schubert, L. W. Tu, G. J. Zydzik, R. F. Kopf, A. Benvenuti, and M. R. Pinto, "Elimination of heterojunction band discontinuities by modulation doping," *Appl. Phys. Lett.*, vol. 60, no. 4, pp. 466–468, 1992.

[15] K. Kurihara, T. Numai, I. Ogura, A. Yasuda, M. Sugimoto, and K. Kasahara, "Reduction in the series resistance of the distributed Bragg reflector in vertical cavities by using quasi-graded superlattices at the heterointerfaces," *J. Appl. Phys.*, vol. 73, no. 1, pp. 21–27, 1993.

[16] N. Tansu and L. J. Mawst, "Current injection efficiency of InGaAsN quantum-well lasers," *J. Appl. Phys.*, vol. 97, no. 5, pp. 054502-1–054502-18, 2005.

[17] C. Z. Tong, S. F. Yoon, C. Y. Ngo, C. Y. Liu, and W. K. Loke, "Rate equations for 1.3 μm dots-under-a-well and dots-in-a-well selfassembled InAs/GaAs quantum dot lasers," *IEEE J. Quantum Electron.*, vol. 42, no. 11, pp. 1175–1183, Nov. 2006.

[18] F. Toor, D. L. Sivco, and C. F. Gmachl, "Effect of waveguide side-wall roughness on the performance of quantum cascade lasers," in *Proc. SPIE*, vol. 7230. 2009, p. 72301P.

[19] B. W. Hakki and T. L. Paoli, "Gain spectra in GaAs double-heterostructure injection lasers," *J. Appl. Phys.*, vol. 46, no. 3, pp. 1299–1306, 1975.

[20] T. R. Chen, L. Eng, B. Zhao, Y. H. Zhuang, S. Sanders, H. Morkoc, and A. Yariv, "Submilliamp threshold InGaAs-GaAs strained layer quantum-well laser," *IEEE J. Quantum Electron.*, vol. 26, no. 7, pp. 1183–1190, Jul. 1990.

[21] A. Tomita and A. Suzuki, "Carrier-induced lasing wavelength shift for quantum well laser diodes," *IEEE J. Quantum Electron.*, vol. 23, no. 7, pp. 1155–1159, Jul. 1987.

[22] G. Hasnain, K. Tai, L. Yang, Y. H. Wang, R. J. Fischer, J. D. Wynn, B. Weir, N. K. Dutta, and A. Y. Cho, "Performance of gain-guided surface emitting lasers with semiconductor distributed Bragg reflectors," *IEEE J. Quantum Electron.*, vol. 27, no. 6, pp. 1377–1385, Jun. 1991.

[23] J. M. T. Pereira, "Self-heating effects at CW operation of MQW long-wavelength lasers," *Mater. Sci. Eng. B*, vol. 74, nos. 1–3, pp. 84–88, 2000.

Cunzhu Tong (M'09) received the Ph.D. degree in microelectronics and solid electronics from the Institute of Semiconductors, Chinese Academy of Sciences, Beijing, China, in 2005.

He joined the Compound Semiconductor and Quantum Information group in the School of Electrical and Electronic Engineering, Nanyang Technological University, Singapore, as a Research Fellow. His research was focused on GaAs-based quantum dot material and devices. Since 2009, he has been a Post-Doctoral Fellow in the Photonics Group, Edward S. Rogers, Sr. Department of Electrical and Computer Engineering, University of Toronto, Toronto, ON, Canada. His current research interests include high-power Bragg reflector waveguide lasers and ultrashort-pulse lasers. He has authored or co-authored nearly 40 refereed journal and conference papers and holds two patents.

Bhavin J. Bijlani was born in Ndola, Zambia, in 1981. He received the Engineering Sciences degree from the University of Toronto, Toronto, ON, Canada, in 2005. He is currently pursuing the Ph.D. degree with the Photonics Group, Edward S. Rogers, Sr. Department of Electrical and Computer Engineering, University of Toronto.

His current research interests include nonlinear frequency conversion and diode lasers in semiconductor Bragg reflection waveguides.

Sanaz Alali received the M.A.Sc. degree in electrical engineering from the Sharif University of Technology, Tehran, Iran, in 2006. She is currently working toward the Ph.D. degree at the University of Toronto, Toronto, ON, Canada.

She is currently with the Edward S. Rogers, Sr. Department of Electrical and Computer Engineering, University of Toronto. Her current research interests include semiconductor diode lasers and nonlinear optical properties in III–V semiconductors.

Amr S. Helmy (M'99–SM'06) received the B.Sc. degree in electronics and telecommunications engineering from Cairo University, Cairo, Egypt, in 1993. He received the M.Sc. and Ph.D. degrees in photonic fabrication technologies from the University of Glasgow, Glasgow, U.K., in 1994 and 1999, respectively.

He was with the Research and Development Division, Agilent Technologies, U.K., where he was engaged in developing distributed feedback lasers, monolithically integrated lasers, modulators, and amplifiers in InP-based semiconductors. He also developed high-powered submarine-class 980-nm InGaAs pump lasers. He is currently an Associate Professor in the Edward S. Rogers, Sr. Department of Electrical and Computer Engineering, University of Toronto, Toronto, ON, Canada. His current research interests include photonic device physics and characterization techniques, with emphasis on nonlinear optics in III–V semiconductors, applied optical spectroscopy in III–V optoelectronic devices and materials, and III–V fabrication and monolithic integration techniques.

Dr. Helmy is a member of the Optical Society of America.